RESEARCH PAPER

Analysis of Ti- and Pb-based particles in the aqueous environment of Melbourne (Australia) via single particle ICP-MS

Raquel Gonzalez de Vega[1,2] · Thomas E. Lockwood[2] · Xiaoxue Xu[3] · Claudia Gonzalez de Vega[2] · Johannes Scholz[2,4] · Maximilian Horstmann[2,4] · Philip A. Doble[2] · David Clases[1,2]

Abstract

The analysis of natural and anthropogenic nanomaterials (NMs) in the environment is challenging and requires methods capable to identify and characterise structures on the nanoscale regarding particle number concentrations (PNCs), elemental composition, size, and mass distributions. In this study, we employed single particle inductively coupled plasma-mass spectrometry (SP ICP-MS) to investigate the occurrence of NMs in the Melbourne area (Australia) across 63 locations. Poisson statistics were used to discriminate between signals from nanoparticulate matter and ionic background. TiO_2-based NMs were frequently detected and corresponding NM signals were calibated with an automated data processing platform. Additionally, a method utilising a larger mass bandpass was developed to screen for particulate high-mass elements. This procedure identified Pb-based NMs in various samples. The effects of different environmental matrices consisting of fresh, brackish, or seawater were mitigated with an aerosol dilution method reducing the introduction of salt into the plasma and avoiding signal drift. Signals from TiO_2- and Pb-based NMs were counted, integrated, and subsequently calibrated to determine PNCs as well as mass and size distributions. PNCs, mean sizes, particulate masses, and ionic background levels were compared across different locations and environments.

Keywords Lead · Nanoparticles · SP ICP-MS · Single particle analysis · Environmental interaction

Introduction

Nanomaterials (NMs) have various properties that are dependent on their size, shape, and composition[1, 2]. They are ubiquitous in the environment, but their effects and functions in natural processes have often been overlooked

✉ David Clases
David.Clases@uni-graz.at

[1] Institute of Chemistry, University of Graz, 8010 Graz, Austria

[2] The Atomic Medicine Initiative, University of Technology Sydney, 15 Broadway, Ultimo, NSW 2007, Australia

[3] School of Biomedical Engineering, University of Technology Sydney, 15 Broadway, Ultimo, NSW 2007, Australia

[4] Institute of Inorganic and Analytical Chemistry, University of Münster, Corrensstr. 48, 48149 Münster, Germany

or ignored due to a lack of analytical tools [2, 3]. NMs are produced on a large scale via natural pathways but also from incidental and intentional anthropogenic processes, and may be grouped into three categories describing their origin: natural, incidental, and engineered [3, 4]. Natural and anthropogenic global fluxes of NMs have been estimated to be hundreds of Tg (10^{12} g) per year [3]. The formation of natural NMs is a complex process that depends on numerous physical and chemical parameters that vary across different environments and times. Weathering, the abundance of precursors, dissolution, redox reactions, precipitation, and aggregation are some of these parameters and may affect the formation and stability of NMs [3]. Incidental NMs have been unintentionally produced since the Industrial Revolution by anthropogenic activities and their abundance may even exceed the levels of naturally occurring NMs in certain areas with high anthropogenic pressure. As new scientific and industrial applications for NMs have emerged in the last century, the production of engineered NMs has increased. Research applications include dedicated drug delivery systems [5], diagnostic imaging [6, 7] and therapeutic agents

[5]. Industrial applications range from electronics, alternative energy sources [8], agriculture [9], coatings and paints [10].

Dedicated procedures are required to identify and further investigate the abundances, sizes, shapes, composition, and reactivities of NMs [2, 3] to understand their environmental behaviour and fate. While some NMs may have been vital in the geological history of the earth and even for the origin of life [3, 11–13], others may have an adverse impact on ecology and health [14]. Specifically, the abundance and effects of suspended NMs in surface waters and the oceans are highly relevant, but remain mostly unexplored. Furthermore, environmental systems are complex and the exact behaviours and reactions of NMs within environmental matrices are difficult to predict obscuring knowledge of types, rates, and extent of transformations as well as associated risks [15].

The analysis of suspended NMs in surface and oceanic waters requires analytical methods that are capable of analysing large sample sets and volumes in complex matrices, while providing efficient NM counting and models of elemental compositions, sizes and/or masses. Techniques like scanning (SEM) or transmission electron microscopy (TEM) with energy-dispersive x-ray analysis (EDX) are suitable to investigate the morphology and elemental composition of individual NMs but are limited for the determination of number concentrations and the construction of larger representative models of size distributions, and matrix- or particle-particle interactions. Surface processes and the charge of particles can be described using a zeta potentiometer, and the hydrodynamic diameter by dynamic light scattering and nanoparticle tracking. Further methods that are relevant for the characterisation of NMs include size exclusion chromatography and flow-field flow fractionation which were used to perform size separations. A summary and comparison of techniques for the characterisation of NMs can be found in a review by Mourdikoudis et al. [2].

Mass spectrometry has emerged as a promising alternative for the characterisation of NMs and, specifically, inductively coupled plasma-mass spectrometry (ICP-MS) enables advanced NM characterisation. ICP-MS was developed approximately 40 years ago and is a platform technology for the sensitive analysis of most elements of the periodic table. In ICP-MS, a hot Ar plasma is used as atomisation and ionisation source to produce elemental ions which are subsequently extracted, mass-filtered, and detected. The hyphenation of ICP-MS with secondary instrumentation such as chromatography and laser ablation (LA) has expanded the capabilities of ICP-MS further by providing speciation data [16] and spatial distributions of elements [17]. Application of rapid mass analysers enabled the detection of discrete particles when NMs are introduced into the plasma individually [18]. In this so-called single particle (SP) ICP-MS, each NM produces a spatially secluded ion cloud, which

is extracted, analysed, and detected individually as a single pulse. The underlying methodology was introduced and gradually advanced over the last two decades [19–21], and was further applied to the analysis of micrometre-scaled particles like microplastics [22, 23]. Recent application to unicellular organisms has led to the development and refinement of methods collectively known as single cell ICP-MS [22, 24, 25]. The frequency of detected pulses is proportional to the number concentration of particles, and the pulse intensity is proportional to the targeted isotope mass. The introduction of rapid mass analysers enabled the reduction of dwell times from milliseconds to microseconds to detect extracted ion clouds from individual particles with several data points, thereby improving accuracy and signal to noise ratios [26–28]. The quadrupole has emerged as a frequently applied mass analyser, which however limits the number of investigated *m/z* to 1 per NM. An elegant and more recent technology to acquire multiple elements in a single NM is SP ICP-ToF (time-of-flight)-MS, which also offers rapid signal acquisition and improved mass resolution [29]. This is useful for screening NMs and in-depth characterisations [30, 31]. Praetorius et al. [32] and Loosli et al. [33] demonstrated that SP ICP-ToF-MS improved the characterisation of suspended NMs and were able to distinguish between natural and engineered NMs by comparing elemental compositions of particles. Similarly, Azimzada et al. [34] described the global abundance and composition of Ti-, Ce-, and Ag-based NMs. The performance of ICP-MS can also be improved via sector-field ICP-MS and ICP-MS/MS. While the former may increase mass resolution and as such improve the selectivity and sensitivity especially for interfered isotopes in SP analysis [35], it is often employed for its higher ion transmission rather than increased mass resolution [36, 37]. ICP-MS/MS may be used to exploit chemical affinities and reactions mitigating spectral interferences and improving figures of merit for interfered isotopes [38].

Altogether, SP ICP-MS offers unique strategies for the analysis and counting of individual NMs while providing high sample throughput. Dedicated models may also be constructed to describe number and size distributions, particle-particle interactions, and to differentiate between ionic and particulate analytes [39]. SP ICP-MS has previously been applied to investigate the levels and sizes of NMs in the environment. For example, Loosli et al. [33] analysed TiO_2 NMs following sewage spills; Gondikas et al. [40] detected and quantified particles in surface waters; and Sanchis et al. [41] investigated the occurrence of CeO_2, Ag, and TiO_2 NMs in river water.

This study employed SP ICP-MS to investigate NMs in environmental waters surrounding Melbourne, a major metropolis in Australia. Samples were sourced from different locations in and around the city including rivers, ports, and lakes within proximity to major facilities such as airports,

industrial grounds, and wastewater treatment plants. Aside from Ti as previously reported NMs, a screening method for SP ICP-MS employing a quadrupole mass analyser with a large mass bandpass was developed to pinpoint particulate elements in the high mass range. This procedure identified particulate Pb in various samples, and particle number concentrations (PNCs), size and elemental mass distributions, figures of merit, and the ionic background across the courses of major rivers were determined.

Materials and methods

Chemicals and consumables

Ultra-pure water was obtained from an Arium Pro system (Sartorius Lab Instruments GmbH & Co., KG, Germany). Elemental standards for ICP-MS were purchased at 10 µg mL^{-1} from Choice Analytical (Thornleigh, NSW, Australia). The detector deadtime was determined and compensated following the analysis of a diluted Er standard. The daily performance of the ICP-MS instrumentation was monitored and optimised by analysing a tuning solution containing 1 ng mL^{-1} Li, Y, Tl, Ce, and Ba. A 15 ± 1.3 nm Au NP dispersion (NanoXact Nanopheres—Bare, Citrate, 99.99 % purity) was obtained from nanoComposix (CA, USA) in 2 mM sodium citrate solution, stored at 4 °C and sonicated before each use. The characterisation of the Au NPs was undertaken by the manufacturer using ICP-MS and TEM. 0.45-µm PTFE syringe filters were obtained from Tisch Scientific (North Bend, OH, USA).

Instrumentation

An 8900 series ICP-MS system (Agilent Technologies, Santa Clara, CA, USA) was equipped with platinum cones and s-lenses and operated with MassHunter software (Agilent Technologies). A Scott-type double-pass spray chamber (Glass Expansion, West Melbourne, Victoria, Australia) was cooled to 2 °C, and a MicroMist™ concentric nebuliser (Elemental Scientific, Omaha, NE, USA) was used for sample nebulisation. This study investigated samples obtained from river, surface, brackish, and coastal seawater in the catchment of Melbourne (Victoria, Australia). These complex environmental matrices were not immediately compatible with ICP-MS due to the high salt content which causes the deposition of matter on the interface and ion lenses. A high matrix introduction (HMI) accessory was previously found adequate to bypass these issues by performing on-line aerosol dilution between the spray chamber and the torch for robust analysis [22, 42] and was employed to bypass drift while analysing samples with high salt content. A method with an increased mass bandpass further referred to

as bandpass mode was used to screen for particulate species in all samples. Further information on the development and application of the bandpass mode can be found elsewhere [39, 43–45]. TiO$_2$, as frequently reported nanoparticulate entity, and particulate Pb, identified via the bandpass mode, were investigated using a quadrupole dwell time of 0.1 ms (Table S1).

A JEOL2200FS TEM equipped with a QUANTAX EDS was used to characterise the morphology and the elemental composition of NMs in selected samples. The accelerating voltage was 200 kV.

Campaign and sample preparation

The sampling campaign was undertaken from the 9th to the 11th of December 2019 within the catchment of greater Melbourne accommodating more than 5 million inhabitants (Figure 1). The sampling campaign time corresponded to Australian summer and temperatures deviated between 12 and 38 °C. There was no precipitation during the sampling period and no rain was recorded for more than 1 week prior. More information on the weather and tidal season is available in the supporting information (Figure S1). Samples were sourced at 63 different locations in polypropylene containers, frozen, and shipped within 24 h. The impact of freezing was evaluated by comparing the occurrence and mass of particles in representative samples before and after freezing and no significant differences were detected. Before sampling, containers where washed and passivated with the sampling matrix. Upon analysis, samples were thawed, sonicated in a water bath for 10 min at room temperature, and filtered (40 mL total volume) using syringe filters (0.45 µm pore size, PTFE) to remove larger particulate matter. The filtered water was immediately analysed via SP ICP-MS.

SP ICP-MS data acquisition and processing

For the bandpass mode, the quadrupole was operated with a decreased mass resolution which enabled the analysis of several isotopes simultaneously. The bandwidth was tuned to collect any isotopes within mass windows of 8 amu using an acquisition time of 20 s. Six mass windows enabled single particle acquisition of a total of 25 elements with isotopes within the mass range of 139–204 amu in 2 min per sample. If signal spikes corresponding to individual NMs were detected in any mass window, nominal mass resolution was re-established in a second run for identification and further analysis.

Signal thresholding/recognition, accumulation, and calibration were performed with an in-house developed open-source Python-based data processing platform using the libraries PySide2, NumPy, and Bottleneck. Detailed information on thresholding algorithms and calibration pathways
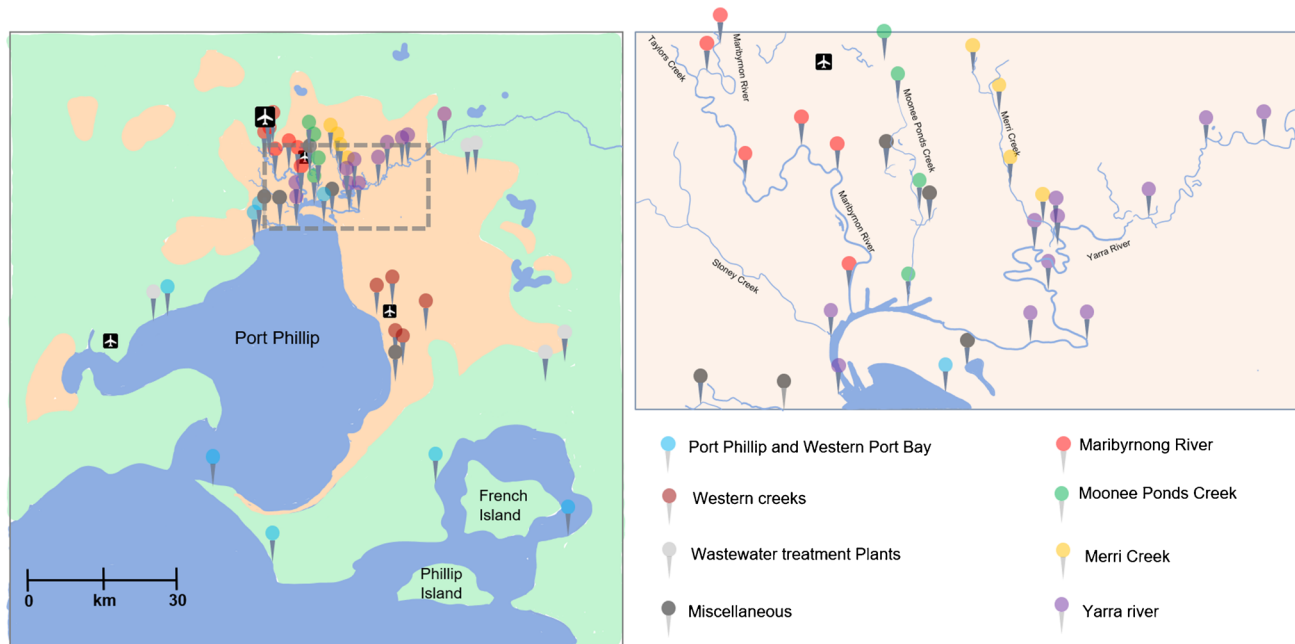
Fig. 1 Sampling locations across the larger Melbourne area. Left: overview of all sample locations within the Melbourne area. Areas indicated in orange correspond to a high population/industrial den-

sity. The metropolitan area of Melbourne (dashed square) is magnified on the right and shows several rivers and the Port Philip estuary

are available elsewhere [46]. Briefly, to distinguish signals of NMs from ionic background and noise, a dynamic Poisson filter was employed. This filter determined the mean signal over 1500 neighbouring data points and determined a threshold over which a signal was considered a NM. Limits of criticality and detection were calculated based on Poisson statistics for paired observations [26, 46, 47]. The transport efficiency (η) was estimated by analysing 15 nm Au NP dispersion and 1 ng/g Au ICP-MS standard diluted in ultra-pure and seawater using an uptake rate of 0.57 mL min^{-1}. The transport efficiency was investigated in pure, sea, and river waters and no significant differences were recorded. Masses, sizes, PNCs, and figures of merit were calculated as reported previously [46].

Results and discussion

Method development and data analysis

Besides targeting Ti-based particles via SP ICP-MS, a bandpass mode was developed to screen for particulate elements in the high mass range. NMs containing elements within the high mass range have previously been described in the environment and may arise from a geogenic origin or anthropogenic discharges [41]. The screening for NMs in environmental matrices with a single collector instrument requires relatively large sample volumes and is time-consuming.

To detect NMs at low PNCs, enough time must be spent on each *m/z* to collect sufficient particles containing the targeted isotope. To accelerate the screening process, the quadrupole mass bandwidth was tuned to be 8 amu and used to identify SP signal signatures from elements with isotopes within defined mass windows between 139 and 204 amu. Six mass windows (139–146 amu, 153–160 amu, 165–172 amu, 175–182 amu, 187–194 amu, and 197–204 amu) allowed screening for 25 elements in each sample. A total acquisition time of 20 s per mass window was used to detect signal spikes in samples. Samples with spikes were subsequently reanalysed with nominal mass resolution to identify the particulate element and to perform PNC, size, and mass calibrations. This approach enabled screening for high-mass elements in 63 samples within approx. 140 min. In addition to the acquisition of several *m/z* simultaneously, the bandpass mode also exhibited a higher ion transmission which improved the detection of small/light NMs as described elsewhere [39].

Water samples were collected along the course of major rivers in the Melbourne area. These rivers had estuaries in the Port Phillip Bay and transitioned from freshwater to brackish water, which complicated the analysis by SP ICP-MS. Complex matrices such as brackish water may be problematic due to the high abundance of matrix ions causing signal drift via space charge effects and salt deposition on the vacuum interface and ion lenses. The robust analysis of all samples with a common method required dilution to

limit the salt burden in the plasma. One common strategy to mitigate matrix effects is the off- or on-line dilution with pure water. However, this may affect the stability of NMs, specifically the particle-particle and matrix-particle interactions. For example, changing the matrix composition may alter the adsorption of ionic analytes on the surface of NMs. Therefore, an on-line aerosol dilution system (HMI) was used to dilute already nebulised samples between spray chamber and plasma with an additional Ar gas flow. The robustness of this method was evaluated by repeatedly analysing and calibrating the size of an Au NP standard diluted in filtered coastal seawater over 90 min (compare Figure S2). The (size) drift rate was estimated to be 0.0354 % min^{-1} (compare Figure S2) using a linear fit and demonstrated the ability to perform robust analysis and calibration. However, the on-line aerosol dilution reduced the transport efficiency to between 0.14 and 0.36 %, which may limit the application of the HMI system to samples with sufficiently high PNCs.

Interferences for Ti isotopes were reduced by employing a mass shifting method and targeting $^{48}Ti^{16}O$ via SP ICP-MS/MS. Operating a mass analyser with short dwell times led to low background counting rates which could be modelled with a Poisson filter as previously discussed elsewhere [22, 26, 47]. Here, a dynamic Poisson filter was used to determine mean values across 1500 data points, from which limits of detection (blue line in Figure 2A) and criticality (green line in Figure 2A) were estimated based on Poisson statistics [46]. Signals exceeding the limits of detection (marked with red square) were summed for values above the limits of criticality and saved in a data array for size and mass calibration. In case of Ti, it was assumed that NMs were present as TiO$_2$ to estimate the spherical diameter as shown in Figure 2B.

Mass distributions may be calibrated as shown in Figure 2C. The screening method revealed a high abundance of Pb-containing NMs (Figure 3A). The properties of these NMs (e.g., density and Pb mass fraction) were unknown, and as such, mass calibration was preferred over size calibration. Two theories were considered for the occurrence of these NMs and are discussed in greater detail below; NMs may either consist of discrete insoluble Pb (e.g., PbO), which may originate from natural or incidental processes, or they may consist of ionic Pb accumulating on the surfaces of other nano-scaled particulate matter such as SiO$_2$, TiO$_2$, carbon or Al$_2$O$_3$. The latter theory was more plausible given that high levels of Pb were previously described in the investigated region and that ionic Pb tends to adsorb on sediments and larger particulate matter [48, 49]. The mass of Pb per particle can be calculated as shown in Figure 3B. The resulting distributions can further be translated into the number of Pb ions per NM as shown in the same figure but on the opposite x-axis. In this case, the PNC detection limit was assessed by analysing three blank solutions and applying the Poisson filter for signal recognition. The average background TiO$_2$ and Pb particle count was 4.0 ($\pm$ 2.9) and 5.3 ($\pm$ 2.9) respectively, and only samples with significantly (3σ) higher count rates were reported.

Pb adsorption on nanomaterials

High levels of Pb have previously been described in soils and sediments in the metropolitan area of Melbourne [48, 50, 51] and are the legacy of urban development and industrial activities but may also be attributed to geogenic backgrounds. Previous studies have investigated the levels of Pb

Fig. 2 **A** SP ICP-MS/MS data monitoring $^{48}Ti^{16}O$ in a selected environmental sample. A Poisson filter was used to identify signals from NMs. **B** Detected signals were calibrated into TiO$_2$ sizes and displayed in a histogram to visualise the size distribution. **C** Ti mass distribution across individual particles
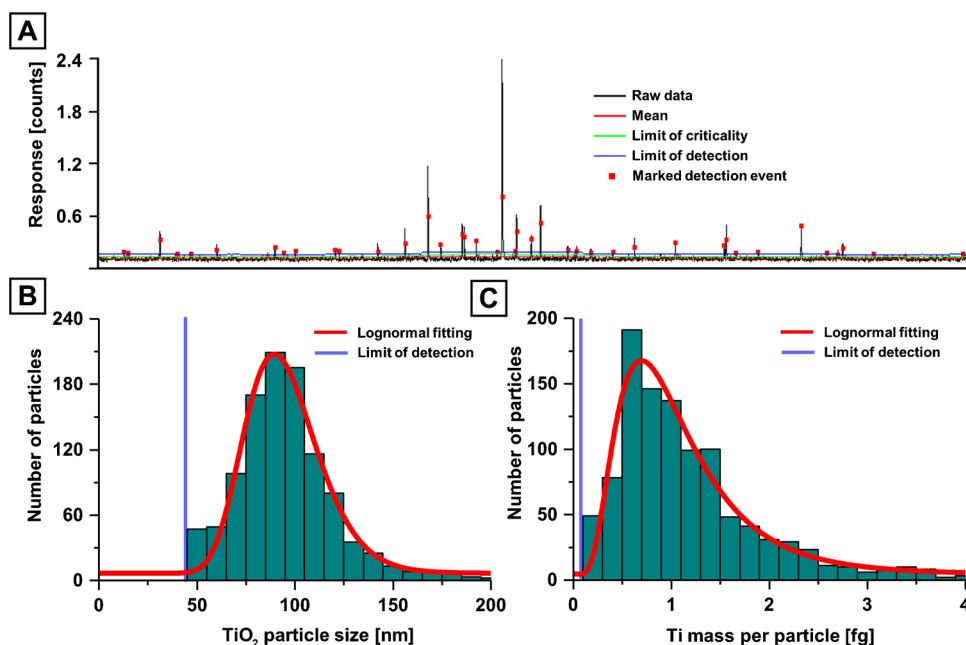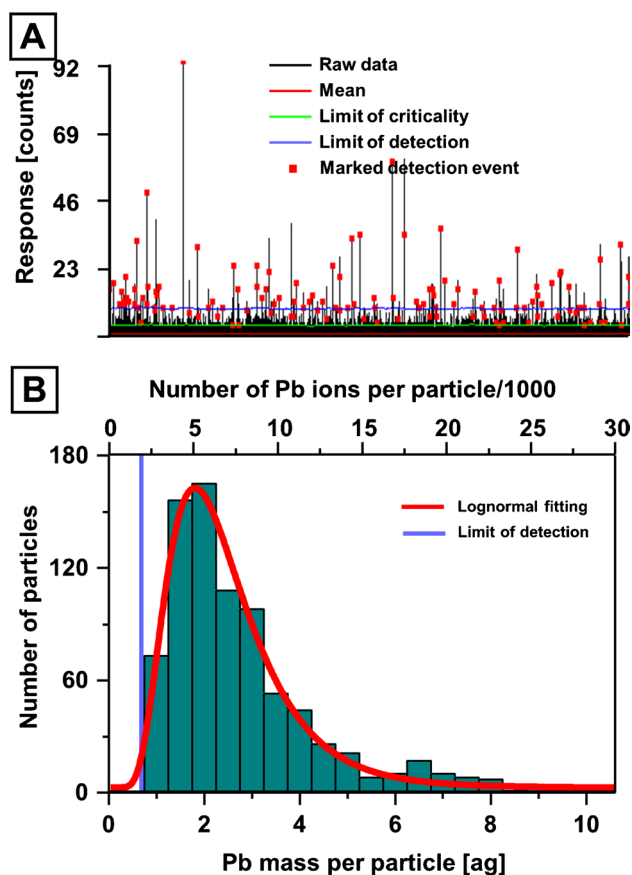
Fig. 3 **A** Transient analysis of ^{208}Pb. **B** Using the thresholding and calibration approach, signals were recognised and calibrated into a Pb mass distribution and the number of Pb ions per particle

and its binding to particulate matter and demonstrated that a majority of Pb is bound to particles with sizes exceeding 400 nm [49, 52]. Nevertheless, little is known about the interaction of Pb with smaller nanoparticulate matter. One approach to investigate the adsorption of Pb to NMs is the application of flow-field flow fractionation coupled to ICP-MS as demonstrated by Loosli et al. [53]. However, if sufficient mass is accumulated, SP ICP-MS is applicable to study the adsorbed Pb across individual particles and to establish distribution models as demonstrated in this study. The adsorption of Pb on NMs was investigated after filtering samples with a 450 nm mesh to remove larger particles. To avoid the disruption of chemical equilibria, no further sample treatment was conducted and dilution was performed via the HMI system. This was crucial to control the introduction of environmental matrices into the plasma and to avoid signal drift. It was observed that Pb-containing NMs were most abundant in fresh water, with PNCs decreasing significantly as the freshwater mixed with salt water. Figure 4 shows the SP ICP-MS analysis of Pb-containing NMs in two representative samples obtained from the Yarra River system. Upstream, the Yarra River consists solely of

freshwater but blends with seawater after flowing past a weir (Dights Falls, red bar in Figure 4E). Figure 4A and D compare the SP ICP-MS raw data for a selected pair of up- and downstream water samples (approximate location indicated in Figure 4E). While no discrete signals for Pb-containing NMs were detected in brackish water (downstream sample, Figure 4D), the freshwater sample (upstream sample, Figure 4A) contained several detectable signals corresponding to individual NMs. Sea- and brackish water have matrices with a high ion strength and may change the stability of dispersed NMs by altering their surface potentials and impacting the equilibrium between free and adsorbed ionic species. This may cause either the agglomeration of formerly stable NMs or the complete desorption of ionic Pb from the surface of NMs. To investigate the impact of seawater on the stability of Pb-containing NMs, the upstream sample was diluted in pure and seawater (1:2 v/v) as shown in Figure 4B and C, respectively. It was evident that the dilution in seawater resulted in the removal of Pb-containing NMs; however, they were still detectable after dilution in pure water. Interestingly, dilution in pure water did not only decrease the PNC, but also the signal intensity indicating that the dilution process caused a desorption of Pb from NMs. On the one hand, this supports the hypothesis that ionic Pb was adsorbed reversibly on nano-scaled particles, and on the other hand, it reinforces the requirement to apply aerosol dilution instead of matrix dilution.

The binding of Pb species to NMs is relevant for the mobility of Pb in the environment and may also have eco-toxicological implications. It has previously been shown that heavy metals may accumulate on vector NMs which then promote their bioavailability. For example, Wang et al. [54] demonstrated that the adsorption of Cd on TiO_2 NMs has a transgenerational reproductive toxicity using *Caenorhabditis elegans* as model organism. Heavy metals may accumulate on the surface of NMs, desorb following ingestion by biota, bioaccumulate, and translocate within an organism. To investigate potential NM substrates, TEM/EDX was employed to investigate selected samples and identified TiO_2 as well as SiO_2-based particles as shown for two representative samples in Figures S3 and S4.

Ti and Pb nanomaterials in the environment

The application of SP ICP-MS identified the presence of NMs in 78 % of the investigated samples, 76.5 % contained Ti-based NMs, and Pb-containing NMs were found in 53 % of the samples. As a general trend, it was observed that PNCs and mean Pb masses per particle decreased with increasing saltwater content. All calibrated PNCs, size, or mass distributions are listed with the corresponding ionic background concentration and the limits of detection in Table S2. One potential spectral interference that cannot be fully mitigated
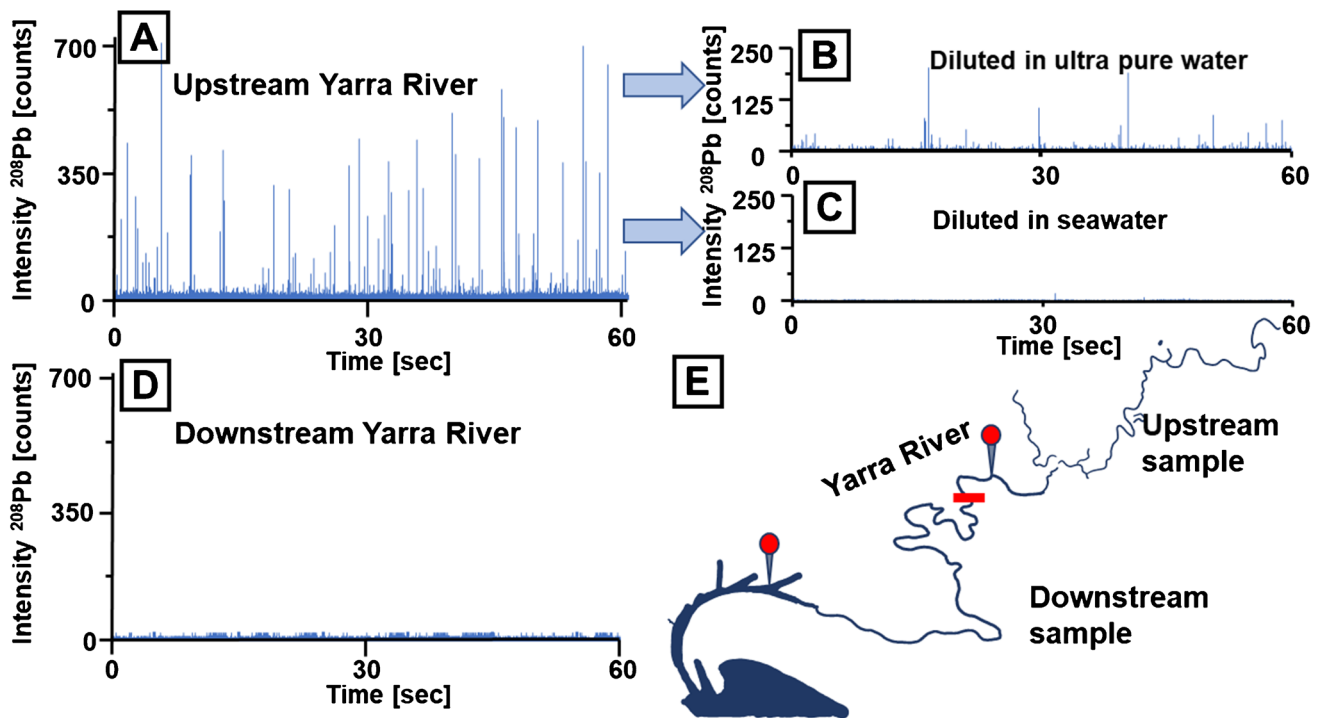
Fig. 4 **A** SP ICP-MS raw data for the isotope [208]Pb. Signal intensities decreased after dilution in **B** pure water and disappear in **C** seawater. **D** SP ICP-MS raw data for [208]Pb in a sample containing brackish water. **E** Scheme of the Yarra River. Sampling locations and the weir are indicated

using an oxygen-based mass shifting methods was Ca ([48]Ca $\rightarrow$ [48]Ca[16]O) [55]. Consequently, the accuracy of determined ionic background may be impacted by high natural Ca levels. The mass detection limit for particulate Pb deviated from 0.8 to 5.7 ag and the size detection limit of TiO_2 particles ranged from 24.4 to 72.5 nm depending on the ionic background levels. The highest PNCs detected were $395 \cdot 10^6$ particles L^{-1} for Pb-containing NMs and $14,600 \cdot 10^6$ particles L^{-1} for Ti-based NMs. The highest mean mass of particulate Pb was 117 ag and the largest detected mean size of TiO_2 was 142 nm. The average size of TiO_2 across all sampling locations was 79.8 nm, which was larger than sizes previously reported (typically between 40 and 50 nm) elsewhere [41, 53]. The TiO_2 PNCs were generally within a range reported across various metropoles in a study by Azimzada et al. [34].

The emission of NMs from wastewater treatment plants (WWTPs) was investigated by sourcing water within the proximity of WWTPs' effluents. In two cases, PNCs were compared up- and downstream of WWTP effluents. While in one case, the PNC decreased after the effluent, a significant increase was detected for the second effluent where Ti-based PNCs increased from no detected NMs to $3200 (\pm 116) \cdot 10^6$ particles L^{-1} and the Pb-containing PNCs increased from no detected NMs to $75.6 (\pm 6.1) \cdot 10^6$ particles L^{-1}. Further samples were obtained within the proximity of effluents distributed across Melbourne, and the highest PNCs were calibrated to be $3440 (\pm 120) \cdot 10^6$ and $171 (\pm 9.1) \cdot 10^6$ particles L^{-1} for Ti- and Pb-containing NMs, respectively. Locations and further data are given in Table S2.

There was no significant number of investigated NMs in samples obtained within the Port Phillip Bay however, in the Western Port, one sample returned the highest Ti PNC detected ($14,600 \cdot 10^6$ particles L^{-1}) within this study. The origin of these NMs was not clear but potential sources may be a landfill and quarry within the proximity of the respective location. Waters from lakes, basins, and wetlands were analysed as shown in Figure 5A, and in all cases, Ti-based NMs were detected with PNCs ranging from 164 ($\pm$ 26.3)$\cdot 10^6$ to 2580 ($\pm$ 104)$\cdot 10^6$ particles L^{-1}. Pb-containing NMs were found in three cases with PNCs of up to 395 ($\pm$ 13.9)$\cdot 10^6$ particles L^{-1}. Figure 5B–D show the Ti (bottom) and Pb (top) PNCs, the mean masses/sizes, and the ionic background along the course of three streams in Melbourne. For comparisons, the geographic situation and the sampling locations are shown adjacently to each diagram. In case of the Yarra River (Figure 5B), samples were obtained at the margin of the metropolitan area (upstream) and downstream within the metropolitan area until the estuary located in the Port Phillip Bay (compare river scheme in Figure 5B). It was observed that over the course of the river, PNCs increased systematically within freshwaters. Outliers were caused by other rivers flowing into the Yarra River (locations 2 and 7 (marked with *)). The Yarra River is separated by a weir (Dight Falls, marked with red bar) into a freshwater section
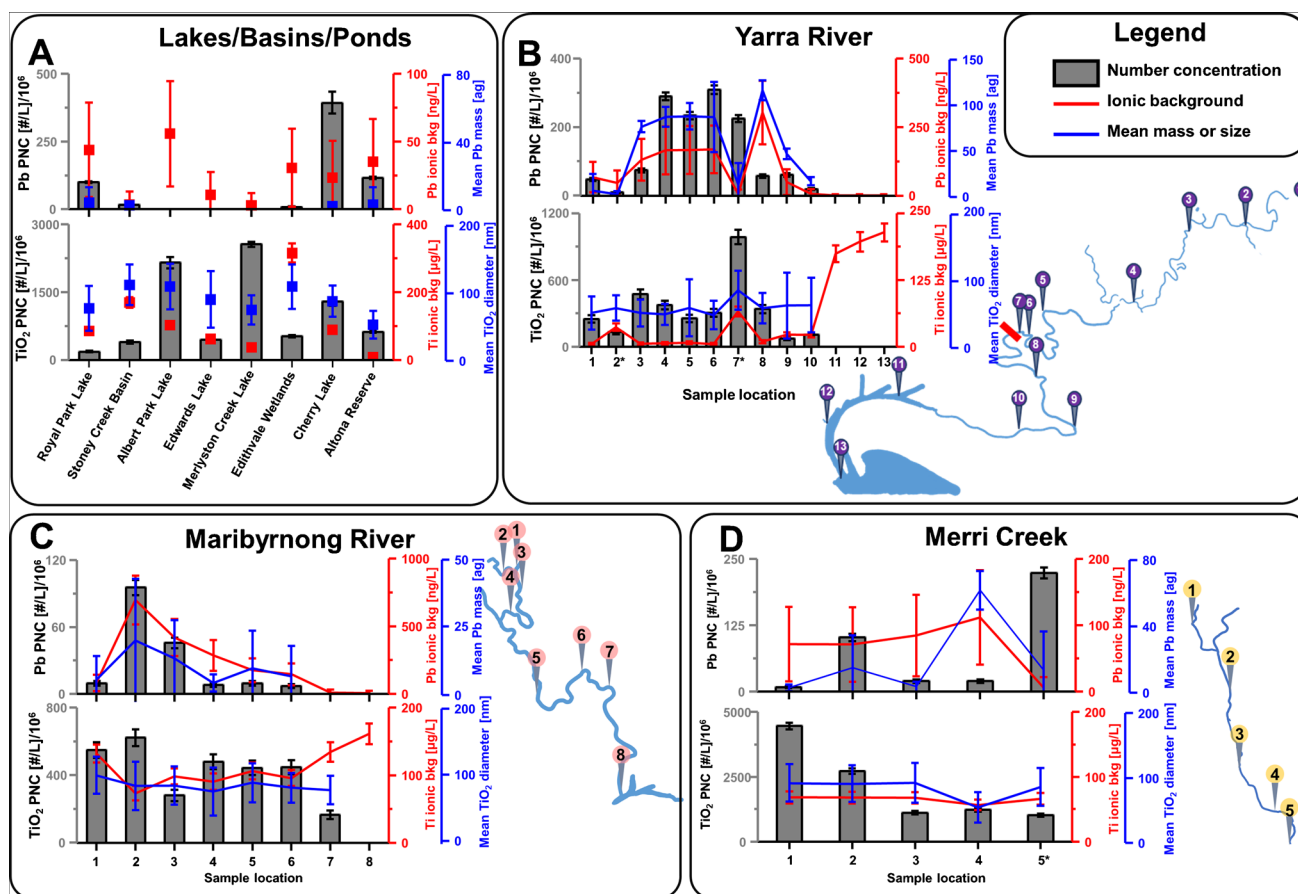
Fig. 5 PNCs, mean sizes and masses, and the ionic background of TiO$_2$ and Pb-containing NMs are shown across different sample locations of Melbourne. **A** Selected lakes and basins. **B** The Yarra River. Sample location 1 is not shown on the map and locations 2 and 7 were in the proximity of inflows of other rivers. **C** Maribyrnong River. **D** Merri Creek

(upstream) and a section that is influenced by tidal seasons and consequently by saltwater (downstream). In the latter section, PNCs decreased substantially. A similar trend was observed for the Maribyrnong River (Figure 5C). For this river, PNCs and sizes of Ti-based NMs were relatively consistent upstream and decreased within the proximity of the Port Phillip Bay. Calibrated ionic Ti background levels were increased in seawater and may be influenced by high ionic Ca levels. Compared against river waters, Ca concentrations are significantly higher in seawater and potentially interfere with selective Ti analysis. Future studies may benefit from alternative mass shifting methods using more selective reaction gases to resolve ^{48}Ca and ^{48}Ti [56].

The highest Pb-containing PNCs were found upstream within the proximity of a major airport and decreased downstream towards Port Phillip Bay, where waters blended with seawater. Figure 5D shows the distribution of NMs across the course of Merri Creek, which is a smaller water stream that flows into the Yarra River shortly before the Dight Falls. Merri Creek transported the highest TiO$_2$ PNC which was

also recognisable at the Yarra River inflow (compare location 7, Figure 5B).

Urban environments are highly dynamic systems with a substantial anthropogenic pressure and further analysis is required in the future to predict the longitudinal and seasonal distribution, the size/mass of NMs as well as their impact on biota. Additionally, the application of SP ICP-ToF-MS may be advantageous to investigate the composition and origin of NMs. As such, the data reported here provides only a snapshot of PNCs, ionic background concentrations, and the masses/sizes of NMs. It is not clear whether the detected concentrations, masses, and sizes pose environmental hazards however, the adsorption of Pb on nanoparticulate matter may be relevant regarding its environmental mobility and bioavailability.

Declarations

References

1. Kolahalam LA, Kasi Viswanath IV, Diwakar BS, Govindh B, Reddy V, Murthy YLN. Review on nanomaterials: synthesis and applications. Mater Today Proc. 2019;18:2182–90. https://doi.org/10.1016/j.matpr.2019.07.371.

2. Mourdikoudis S, Pallares RM, Thanh NTK. Characterization techniques for nanoparticles: comparison and complementarity upon studying nanoparticle properties. Nanoscale. 2018;10:12871–934. https://doi.org/10.1039/C8NR02278J.

3. Hochella MF, Mogk DW, Ranville J, Allen IC, Luther GW, Marr LC, McGrail BP, Murayama M, Qafoku NP, Rosso KM, Sahai N, Schroeder PA, Vikesland P, Westerhoff P, Yang Y (2019) Natural, incidental, and engineered nanomaterials and their impacts on the Earth system. Science (80-). https://doi.org/10.1126/science.aau8299

4. Malakar A, Kanel SR, Ray C, Snow DD, Nadagouda MN. Nanomaterials in the environment, human exposure pathway, and health effects: a review. Sci Total Environ. 2021;759: 143470. https://doi.org/10.1016/j.scitotenv.2020.143470.

5. Fernandez-Fernandez A, Manchanda R, McGoron AJ. Theranostic applications of nanomaterials in cancer: drug delivery, image-guided therapy, and multifunctional platforms. Appl Biochem Biotechnol. 2011;165:1628–51. https://doi.org/10.1007/s12010-011-9383-z.

6. Du Z, Gupta A, Clarke C, Cappadona M, Clases D, Liu D, Yang Z, Karan S, Price WS, Xu X. Porous upconversion nanostructures as bimodal biomedical imaging contrast agents. J Phys Chem C. 2020;124:12168–74. https://doi.org/10.1021/acs.jpcc.0c03945.

7. González de Vega R, Clases D, Fernández-Sánchez ML, Eiró N, González LO, Vizoso FJ, Doble PA, Sanz-Medel A. MMP-11 as a biomarker for metastatic breast cancer by immunohistochemical-assisted imaging mass spectrometry. Anal Bioanal Chem. 2019;411:639–46. https://doi.org/10.1007/s00216-018-1365-3.

8. Jariwala D, Sangwan VK, Lauhon LJ, Marks TJ, Hersam MC. Carbon nanomaterials for electronics, optoelectronics, photovoltaics, and sensing. Chem Soc Rev. 2013;42:2824–60. https://doi.org/10.1039/C2CS35335K.

9. Kopittke PM, Lombi E, Wang P, Schjoerring JK, Husted S. Nanomaterials as fertilizers for improving plant mineral nutrition and environmental outcomes. Environ Sci Nano. 2019;6:3513–24. https://doi.org/10.1039/C9EN00971J.

10. Rasheed PA, Jabbar KA, Mackey HR, Mahmoud KA. Recent advancements of nanomaterials as coatings and biocides for the inhibition of sulfate reducing bacteria induced corrosion. Curr Opin Chem Eng. 2019;25:35–42. https://doi.org/10.1016/j.coche.2019.06.003.

11. Hochella MF, Aruguete D, Kim B, Elwood Madden A. Naturally occurring inorganic nanoparticles: general assessment and a global budget for one of earth's last unexplored major geochemical components. In: Barnard AS, Guo H, editors. Nature's nanostructures. Ltd, Singapore, Singapore: Pan Stanford Publising Pte; 2012. p. 1–42.

12. Sahai N, Kaddour H, Dalai P, Wang Z, Bass G, Gao M. Mineral surface chemistry and nanoparticle-aggregation control membrane self-assembly. Sci Rep. 2017;7:43418. https://doi.org/10.1038/srep43418.

13. Oleson TA, Sahai N, Pedersen JA. Electrostatic effects on deposition of multiple phospholipid bilayers at oxide surfaces. J Colloid Interface Sci. 2010;352:327–36. https://doi.org/10.1016/j.jcis.2010.08.057.

14. Jeevanandam J, Barhoum A, Chan YS, Dufresne A, Danquah MK. Review on nanoparticles and nanostructured materials: history, sources, toxicity and regulations. Beilstein J Nanotechnol. 2018;9:1050–74. https://doi.org/10.3762/bjnano.9.98.

15. Lowry GV, Gregory KB, Apte SC, Lead JR. Transformations of nanomaterials in the environment. Environ Sci Technol. 2012;46:6893–9. https://doi.org/10.1021/es300839e.

16. Bishop DP, Hare DJ, Clases D, Doble PA. Applications of liquid chromatography-inductively coupled plasma-mass spectrometry in the biosciences: a tutorial review and recent developments. Trend Anal Chem. 2018;104:11–21. https://doi.org/10.1016/j.trac.2017.09.017.

17. Doble PA, Gonzalez de Vega R, Bishop DP, Hare DJ, Clases D. Laser ablation–inductively coupled plasma–mass spectrometry imaging in biology. Chem Rev. 2021. https://doi.org/10.1021/acs.chemrev.0c01219.

18. Mozhayeva D, Engelhard C. A critical review of single particle inductively coupled plasma mass spectrometry – a step towards an ideal method for nanomaterial characterization. J Anal At Spectrom. 2020;35:1740–83. https://doi.org/10.1039/C9JA00206E.

19. Degueldre C, Favarger P-Y. Colloid analysis by single particle inductively coupled plasma-mass spectroscopy: a feasibility study. Colloids Surfaces A Physicochem Eng Asp. 2003;217:137–42. https://doi.org/10.1016/S0927-7757(02)00568-X.

20. Degueldre C, Favarger P-Y, Wold S. Gold colloid analysis by inductively coupled plasma-mass spectrometry in a single particle

mode. Anal Chim Acta. 2006;555:263–8. https://doi.org/10.1016/j.aca.2005.09.021.

21. Degueldre C, Favarger P-Y, Bitea C Zirconia colloid analysis by single particle inductively coupled plasma-mass spectrometry. Anal Chim Acta 518:137–142. 101016/jaca200404015

22. Gonzalez de Vega R, Goyen S, Lockwood TE, Doble PA, Camp EF, Clases D. Characterisation of microplastics and unicellular algae in seawater by targeting carbon via single particle and single cell ICP-MS. Anal Chim Acta. 2021;1174: 338737. https://doi.org/10.1016/j.aca.2021.338737.

23. Bolea-Fernandez E, Rua-Ibarz A, Velimirovic M, Tirez K, Vanhaecke F. Detection of microplastics using inductively coupled plasma-mass spectrometry (ICP-MS) operated in single-event mode. J Anal At Spectrom. 2020;35:455–60. https://doi.org/10.1039/c9ja00379g.

24. Theiner S, Loehr K, Koellensperger G, Mueller L, Jakubowski N. Single-cell analysis by use of ICP-MS. J Anal At Spectrom. 2020;35:1784–813. https://doi.org/10.1039/D0JA00194E.

25. Corte-Rodríguez M, Álvarez-Fernández R, García-Cancela P, Montes-Bayón M, Bettmer J. Single cell ICP-MS using on line sample introduction systems: current developments and remaining challenges. TrAC Trends Anal Chem. 2020;132: 116042. https://doi.org/10.1016/j.trac.2020.116042.

26. Mozhayeva D, Engelhard C. A quantitative nanoparticle extraction method for microsecond time resolved single-particle ICP-MS data in the presence of a high background. J Anal At Spectrom. 2019;34:1571–80. https://doi.org/10.1039/C9JA00042A.

27. Strenge I, Engelhard C. Capabilities of fast data acquisition with microsecond time resolution in inductively coupled plasma mass spectrometry and identification of signal artifacts from millisecond dwell times during detection of single gold nanoparticles. J Anal At Spectrom. 2016;31:135–44. https://doi.org/10.1039/C5JA00177C.

28. Abad-Álvaro I, Peña-Vázquez E, Bolea E, Bermejo-Barrera P, Castillo JR, Laborda F. Evaluation of number concentration quantification by single-particle inductively coupled plasma mass spectrometry: microsecond vs. millisecond dwell times. Anal Bioanal Chem. 2016;408:5089–97. https://doi.org/10.1007/s00216-016-9515-y.

29. Meermann B, Nischwitz V. ICP-MS for the analysis at the nanoscale – a tutorial review. J Anal At Spectrom. 2018;33:1432–68. https://doi.org/10.1039/C8JA00037A.

30. Mehrabi K, Günther D, Gundlach-Graham A. Single-particle ICP-TOFMS with online microdroplet calibration for the simultaneous quantification of diverse nanoparticles in complex matrices. Environ Sci Nano. 2019;6:3349–58. https://doi.org/10.1039/C9EN00620F.

31. Borovinskaya O, Hattendorf B, Tanner M, Gschwind S, Günther D. A prototype of a new inductively coupled plasma time-of-flight mass spectrometer providing temporally resolved, multi-element detection of short signals generated by single particles and droplets. J Anal At Spectrom. 2013;28:226–33. https://doi.org/10.1039/C2JA30227F.

32. Praetorius A, Gundlach-Graham A, Goldberg E, Fabienke W, Navratilova J, Gondikas A, Kaegi R, Günther D, Hofmann T, von der Kammer F. Single-particle multi-element fingerprinting (spMEF) using inductively-coupled plasma time-of-flight mass spectrometry (ICP-TOFMS) to identify engineered nanoparticles against the elevated natural background in soils. Environ Sci Nano. 2017;4:307–14. https://doi.org/10.1039/C6EN00455E.

33. Loosli F, Wang J, Rothenberg S, Bizimis M, Winkler C, Borovinskaya O, Flamigni L, Baalousha M. Sewage spills are a major source of titanium dioxide engineered (nano)-particle release into the environment. Environ Sci Nano. 2019;6:763–77. https://doi.org/10.1039/C8EN01376D.

34. Azimzada A, Jreije I, Hadioui M, Shaw P, Farner JM, Wilkinson KJ. Quantification and characterization of Ti-, Ce-, and Ag-nanoparticles in global surface waters and precipitation. Environ Sci Technol. 2021. https://doi.org/10.1021/acs.est.1c00488.

35. Rua-Ibarz A, Bolea-Fernandez E, Pozo G, Dominguez-Benetton X, Vanhaecke F, Tirez K. Characterization of iron oxide nanoparticles by means of single-particle ICP-mass spectrometry (SP-ICP-MS) – chemical versus physical resolution to overcome spectral overlap. J Anal At Spectrom. 2020;35:2023–32. https://doi.org/10.1039/D0JA00183J.

36. Jreije I, Azimzada A, Hadioui M, Wilkinson KJ. Measurement of CeO(2) nanoparticles in natural waters using a high sensitivity, single particle ICP-MS. Molecules. 2020;25:5516. https://doi.org/10.3390/molecules25235516.

37. Fréchette-Viens L, Hadioui M, Wilkinson KJ. Quantification of ZnO nanoparticles and other Zn containing colloids in natural waters using a high sensitivity single particle ICP-MS. Talanta. 2019;200:156–62. https://doi.org/10.1016/j.talanta.2019.03.041.

38. Bolea-Fernandez E, Balcaen L, Resano M, Vanhaecke F. Overcoming spectral overlap via inductively coupled plasma-tandem mass spectrometry (ICP-MS/MS). A tutorial review. J Anal At Spectrom. 2017;32:1660–79. https://doi.org/10.1039/C7JA00010C.

39. Meyer S, Gonzalez de Vega R, Xu X, Du Z, Doble PA, Clases D. Characterization of upconversion nanoparticles by single-particle ICP-MS employing a quadrupole mass filter with increased bandpass. Anal Chem. 2020;92:15007–16. https://doi.org/10.1021/acs.analchem.0c02925.

40. Gondikas A, von der Kammer F, Kaegi R, Borovinskaya O, Neubauer E, Navratilova J, Praetorius A, Cornelis G, Hofmann T. Where is the nano? Analytical approaches for the detection and quantification of TiO2 engineered nanoparticles in surface waters. Environ Sci Nano. 2018;5:313–26. https://doi.org/10.1039/C7EN00952F.

41. Sanchís J, Jiménez-Lamana J, Abad E, Szpunar J, Farré M. Occurrence of cerium-, titanium-, and silver-bearing nanoparticles in the Besòs and Ebro Rivers. Environ Sci Technol. 2020;54:3969–78. https://doi.org/10.1021/acs.est.9b05996.

42. Barros AI, Pinheiro FC, Amaral CDB, Lorençatto R, Nóbrega JA. Aerosol dilution as a simple strategy for analysis of complex samples by ICP-MS. Talanta. 2018;178:805–10. https://doi.org/10.1016/j.talanta.2017.10.024.

43. Clases D, Gonzalez de Vega R, Funke S, Lockwood TE, Westerhausen M, Taudte RV, Adlard PA, Doble P. Matching sensitivity to abundance: high resolution immuno-mass spectrometry imaging of lanthanide labels and endogenous elements in the murine brain. J Anal At Spectrom. 2020;35:728–35. https://doi.org/10.1039/C9JA00405J.

44. Horstmann M, Gonzalez de Vega R, Bishop DP, Karst U, Doble P, Clases D. Determination of gadolinium MRI contrast agents in fresh and oceanic waters of Australia employing micro-solid phase extraction, HILIC-ICP-MS and bandpass mass filtering. J Anal At Spectrom. 2021;36:767–75. https://doi.org/10.1039/D0JA00493F.

45. Bishop DP, Clases D, Fryer F, Williams E, Wilkins S, Hare DJ, Cole N, Karst U, Doble PA. Elemental bio-imaging using laser ablation-triple quadrupole-ICP-MS. J Anal At Spectrom. 2016;31:197–202. https://doi.org/10.1039/C5JA00293A.

46. Lockwood TE, de Vega R, Clases D. An interactive Python-based data processing platform for single particle and single cell ICP-MS. J Anal At Spectrom. 2021;36:2536–44. https://doi.org/10.1039/D1JA00297J.

47. Tanner M. Shorter signals for improved signal to noise ratio, the influence of Poisson distribution. J Anal At Spectrom. 2010;25:405–7. https://doi.org/10.1039/b921077f.

48. Laidlaw MAS, Alankarage DH, Reichman SM, Taylor MP, Ball AS. Assessment of soil metal concentrations in residential and community vegetable gardens in Melbourne, Australia. Chemosphere. 2018;199:303–11. https://doi.org/10.1016/j.chemosphere.2018.02.044.

49. Talbot V. Mobility and speciation of cadmium and lead in polluted seawater of Port Phillip Bay, Australia: management implications. J Coast Res. 1989;5:755–63.

50. Laidlaw MAS, Gordon C, Ball AS. Preliminary assessment of surface soil lead concentrations in Melbourne, Australia. Environ Geochem Health. 2018;40:637–50. https://doi.org/10.1007/s10653-017-0010-y.

51. Mikkonen HG, Clarke BO, Dasika R, Wallis CJ, Reichman SM. Assessment of ambient background concentrations of elements in soil using combined survey and open-source data. Sci Total Environ. 2017;580:1410–20. https://doi.org/10.1016/j.scitotenv.2016.12.106.

52. Hart BT, Davies SHR. Trace metal speciation in the freshwater and estuarine regions of the Yarra River, Victoria. Estuar Coast Shelf Sci. 1981;12:353–74. https://doi.org/10.1016/S0302-3524(81)80001-1.

53. Loosli F, Yi Z, Wang J, Baalousha M. Dispersion of natural nanomaterials in surface waters for better characterization of their physicochemical properties by AF4-ICP-MS-TEM. Sci Total Environ. 2019;682:663–72. https://doi.org/10.1016/j.scitotenv.2019.05.206.

54. Wang J, Nie Y, Dai H, Wang M, Cheng L, Yang Z, Chen S, Zhao G, Wu L, Guang S, Xu A. Parental exposure to TiO2 NPs promotes the multigenerational reproductive toxicity of Cd in Caenorhabditis elegans via bioaccumulation of Cd in germ cells. Environ Sci Nano. 2019;6:1332–42. https://doi.org/10.1039/C8EN01042K.

55. Balcaen L, Bolea-Fernandez E, Resano M, Vanhaecke F. Accurate determination of ultra-trace levels of Ti in blood serum using ICP-MS/MS. Anal Chim Acta. 2014;809:1–8. https://doi.org/10.1016/j.aca.2013.10.017.

56. Candás-Zapico S, Kutscher DJ, Montes-Bayón M, Bettmer J. Single particle analysis of TiO2 in candy products using triple quadrupole ICP-MS. Talanta. 2018;180:309–15. https://doi.org/10.1016/j.talanta.2017.12.041.